Supplementary Information (SI) for Journal of Materials Chemistry C.

Cuprous-Based Layered Single-Crystalline Scintillators for X-ray Detection and Imaging

Yuke Zhao[1,3], Danping Chen[2], Haitao Tang[1,3], Hailin Liu[1], Yong Liu[1],
Yangyang Dang[2,*] and Qianqian Lin[1,3,*]

[1] Key Lab of Artificial Micro- and Nano-Structures of Ministry of Education of China, School of Physics and Technology, Wuhan University, Wuhan 430072, China.

[2] School of Physics and Physical Engineering, Qufu Normal University, Qufu 273165, China.

[3] Hubei Luojia Laboratory, Wuhan 430072, China.

Corresponding Authors:

*Email: q.lin@whu.edu.cn ; dyy@qfnu.edu.cn

1. Experimental Details

Materials: Cuprous iodide (CuI, 99%), hypophoaphoeous acid (H_3PO_2, 50 wt.% in H_2O) and 1,4-phenylenediamine ($C_6H_8N_2$, 97%) were purchased from Aladdin (Shanghai, China). Hydriodic acid (HI, 55%-58%) were purchased from Meryer (Shanghai, China). N,N-dimethyl formamide (DMF, 99.9%) were purchased from Sigma-Aldrich. And acetonitrile (ACN, 99.5%) were purchased from HuShi (Shanghai, China). All of these chemical agents were used without further purification.

Materials Synthesis: CuI (1 mmol, 0.192 g) and 1,4-phenylenediamine (1 mmol, 0.108 g) were added to a mixed solution of 0.6 mL of acetonitrile (ACN), 0.6 mL of hydriodic acid (HI) and 0.9 mL of N, N-dimethyl formamide (DMF), then add 0.9 mL of hypophosphorous acid so1lution. The suspension was heated and stirred continuously at 75 °C for about 15 min until it became clear and the temperature is then lowered by 1 °C every hour until it drops to room temperature, where single crystals are slowly precipitated. The crystal structure was determined as $(C_6H_{10}N_2)_2Cu_2I_3(PO_2)_3$ by single crystal X-ray diffraction. Compared with single crystals, the preparation of powders is relatively simple, CuI (1 mmol, 0.192 g) and p-Phenylenediamine (1 mmol, 0.108 g) were added into 2mL acetonitrile, then 0.9 mL hypophosphorous acid was added to the solution and stirred for ~10 min, the powder can be obtained after filtration and drying.

Synthesis of films: For evaluating the RL performance, we fabricated the composite scintillator films by mixing the screened phosphor with the PDMS at the weight ratio of 1:15 uniformly, followed by transferring the mixture into mould. Finally, the film could be shaped in a drying oven at 60°C for 3 hours.

Characterization: Single-crystal X-ray diffraction data were collected on a Bruker D8 advance diffractometer equipped with a CCD detector (graphite-monochromated Mo-Ka radiation, λ= 0.71073 Å) at 293(2) K. *APEX3* software was used for data integration and cell refinements. The crystal was kept at 293(2) K during data collection. Using *Olex2*,[1] the structure was solved with the *Olex2.solve*[2] structure solution program using Charge Flipping and refined with the *XL*[3] refinement package using Least Squares minimization. The absorption spectra were measured with a visible-NIR spectrometer (Lambda 1050+ UV/VIS/NIR Spectrometer). Photoluminescence (PL) spectra were recorded using a Morpho Nova spectrometer. The decay curves were recorded with a time-correlated single-photon counter (PicoQuant GmbH, TimeHarp 260) and excited with a 405 nm picosecond laser (Advanced Laser Diode Systems A.L.S. GmbH, Pilas). The device performance under X-ray irradiation was carried out with a commercially available X-ray tube (SPELLMAN XRB011, tungsten anode, 20 W maximum power output). Photodetectors were placed in a lead shielded box to prevent ionizing radiation leakage and block the external visible lights. The radiation dose rates were carefully calibrated with a commercial dosimeter (Suhe Instrument Technology Co. LTD, XH-3525). For X-ray imaging, X-rays passed vertically through the object, a black baffle and the scintillator wafer in turn. The black baffle blocks leaked visible light and reduces the influence of light reflected from the object on to the scintillator screen. Finally, a CMOS camera with 1,200×1,200 pixels was utilized to acquire X-ray images.

2. Supplementary notes

2.1 MTF measurement

Modulation transfer function (MTF) determines the spatial resolution of imaging system and represents the ability to transfer input signal modulation of spatial frequency relative to its output. A MTF value of 1 indicates the perfect detection of a given spatial frequency. Using slanted-edge method to calculate MTF, we took the Xray images of a sharp edge from a piece of aluminum (thickness: ~1mm). The edge spread function (ESF) was derived by the edge profile, from which we could deduce the line spread function (LSF) by calculating derivative. Finally, the Fourier transform of the LSF defines the MTF, meaning the MTF curves could be calculated as,

$$MTF(v) = F\big(LSF(x)\big) = F\frac{dESF(x)}{dx} \quad , \quad (1)$$

where v is spatial frequency, x is the position of pixels. Due to using different optical system, the position of pixels is defined as follows:

$$x = \frac{N.d}{I_0} \quad , \quad (2)$$

where N is the ordinal number of pixels in X-ray edge image, d is the pixel size (11 μm) and β is optical magnification.

2.2 PLQY calculation

The PLQY can be calculated by the following formula:

$$\eta = \frac{p_c L_b - p_b L_c}{L_a (L_b - L_c)} \quad , \qquad (3)$$

where L_a, L_b, L_c, P_b, and P_c and are the integral values of L and P for experiments a, b, and c of **Figure S3**, respectively.

3. Supporting figures

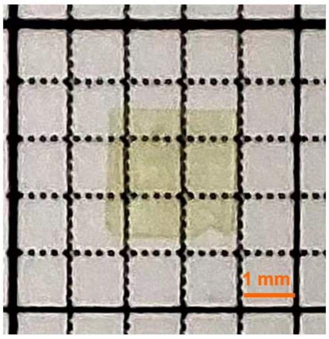

Figure S1 Photo of $(C_6H_{10}N_2)_2Cu_2I_3(PO_2)_3$ single crystal.

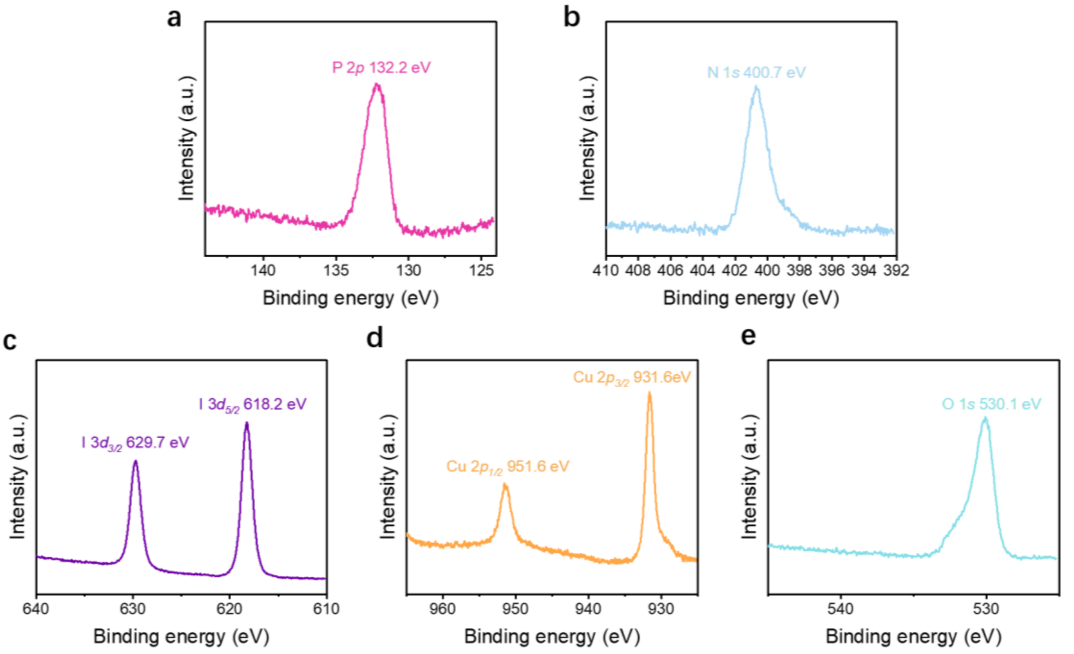

Figure S2 High-resolution XPS spectra of **(a)** P 2*p*, **(b)** N 1*s*, **(c)** I 3*d*, **(d)** Cu 2*p*, **(e)** O 1*s* in $(C_6H_{10}N_2)_2Cu_2I_3(PO_2)_3$ single crystals.

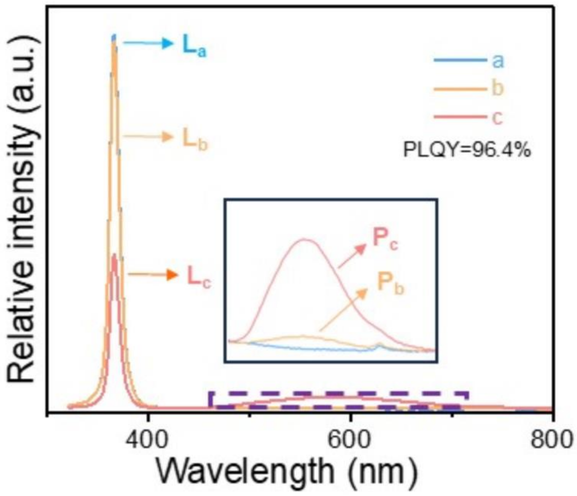

Figure S3 Emission spectra during PLQY measurement in the absence and presence of $(C_6H_{10}N_2)_2Cu_2I_3(PO_2)_3$ under 365 nm excitation. L and P stand for the laser peak and photoluminescence peak of the obtained PL spectra obtained under **a** (integrating sphere without sample), **b** (laser pointed to the wall of integrating sphere and excite samples indirectly) and **c** (laser excite sample directly) conditions.

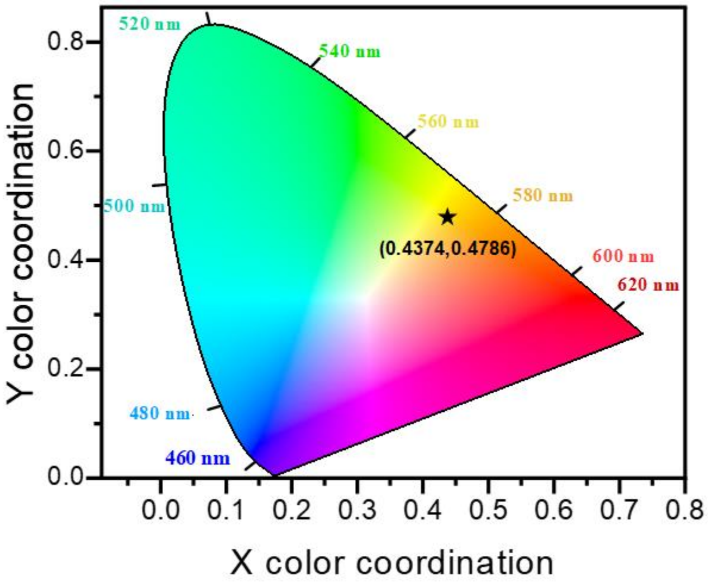

Figure S4 CIE coordinates of $(C_6H_{10}N_2)_2Cu_2I_3(PO_2)_3$.

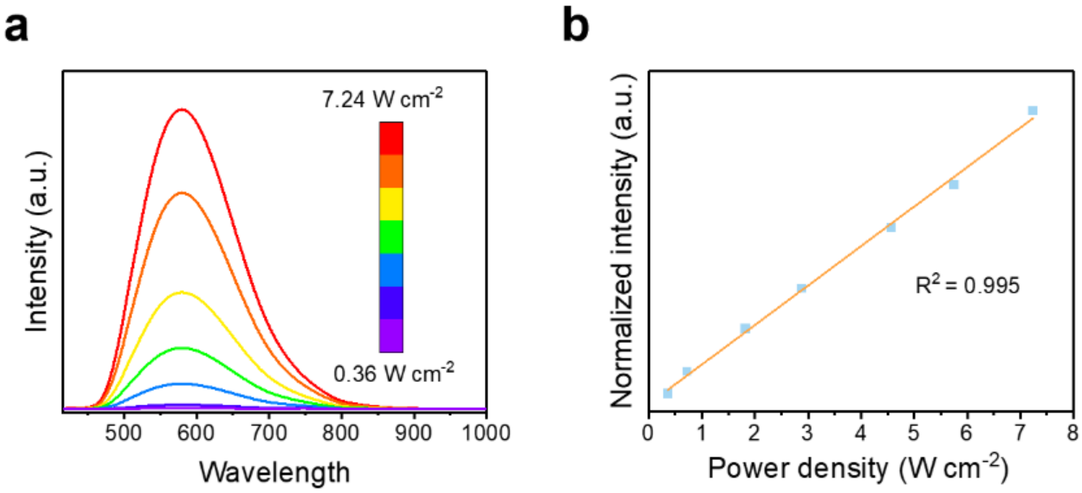

Figure S5 (a) Light intensity dependent PL spectra and **(b)** excitation dependent PL intensity.

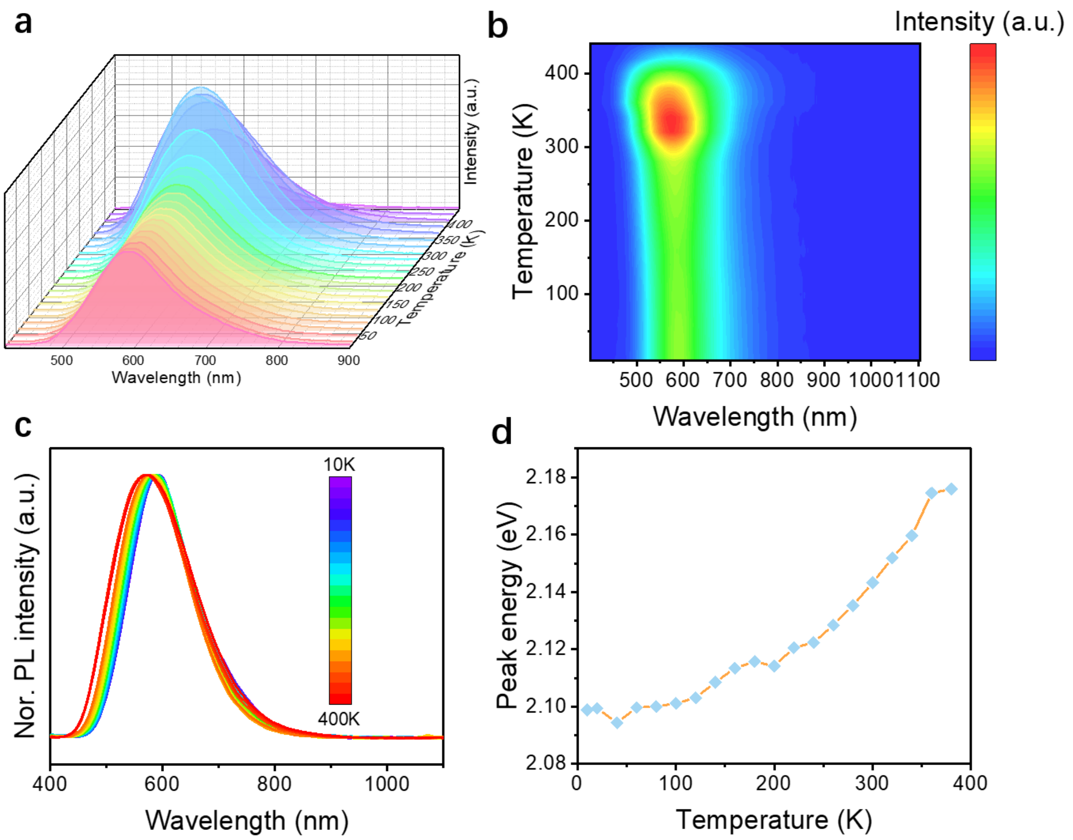

Figure S6 (a) Temperature-dependent PL spectra of $(C_6H_{10}N_2)_2Cu_2I_3(PO_2)_3$ upon 254 nm excitation along with temperature range from 10 to 400 K and temperature interval of 20 K. **(b)** Color mapping of temperature-dependent PL emission spectra. **(c)** Temperature-dependent PL spectra of $(C_6H_{10}N_2)_2Cu_2I_3(PO_2)_3$ after normalized. **(d)** Peak energy of $(C_6H_{10}N_2)_2Cu_2I_3(PO_2)_3$ emissions as a function of temperature.

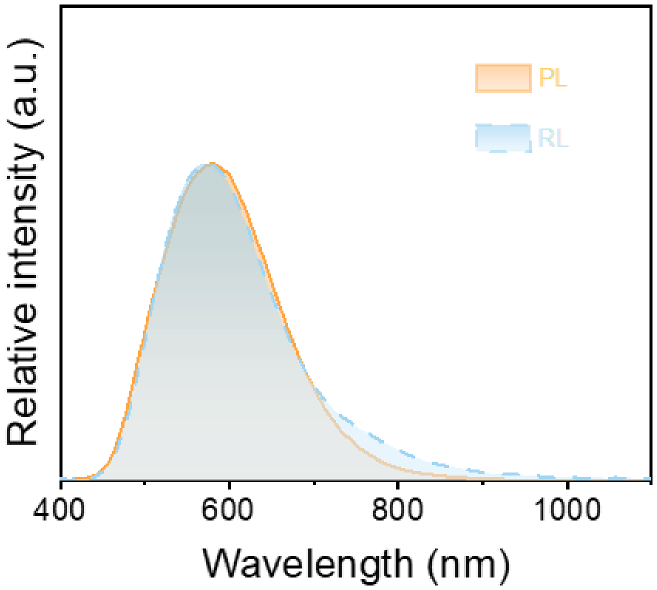

Figure S7 Comparison of the RL and PL spectra of $(C_6H_{10}N_2)_2Cu_2I_3(PO_2)_3$.

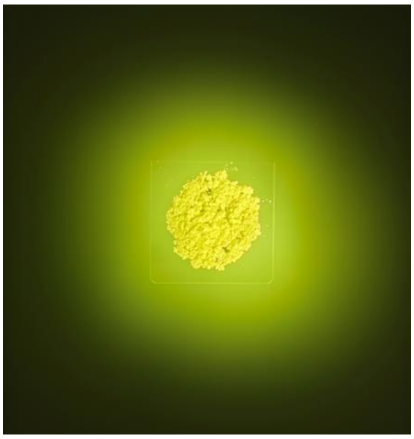

Figure S8 Luminescent photos of the $(C_6H_{10}N_2)_2Cu_2I_3(PO_2)_3$ powder under X-ray irradiation.

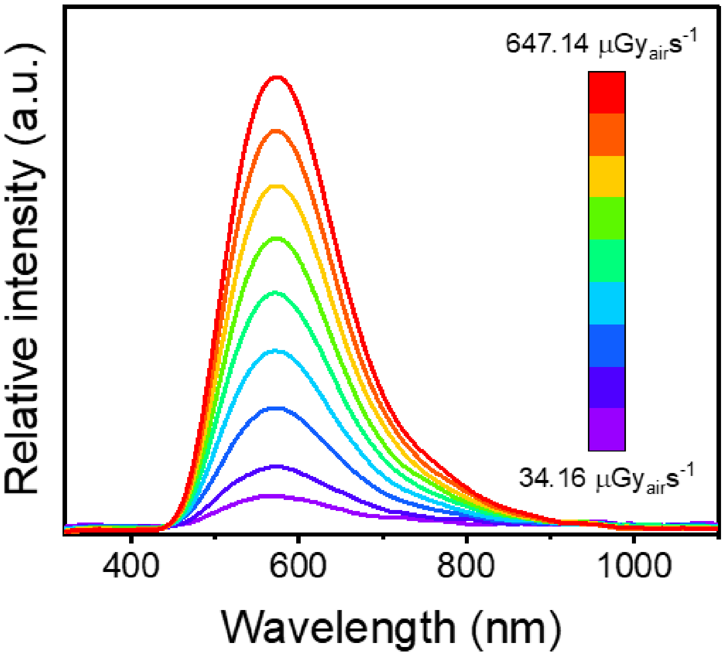

Figure S9 RL spectra of $(C_6H_{10}N_2)_2Cu_2I_3(PO_2)_3$ with variable dose rates from 34.16 μGy$_{air}$ s^{-1} to 647 μGy$_{air}$ s^{-1}.

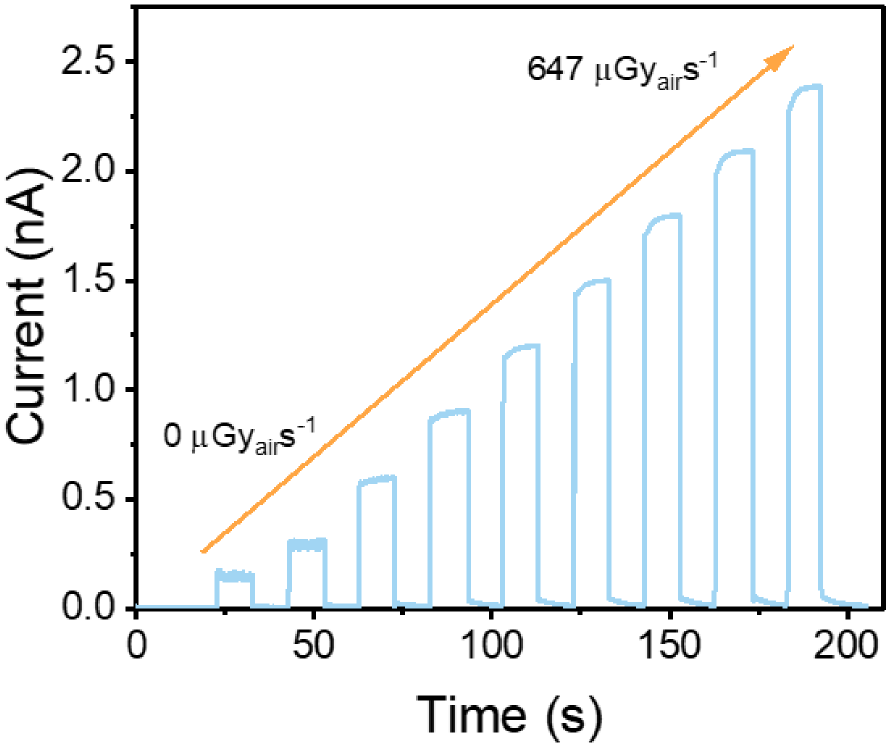

Figure S10 The X-ray response of $(C_6H_{10}N_2)_2Cu_2I_3(PO_2)_3$ with variable dose rates from 0 to 647 μGy$_{air}$ s^{-1}.

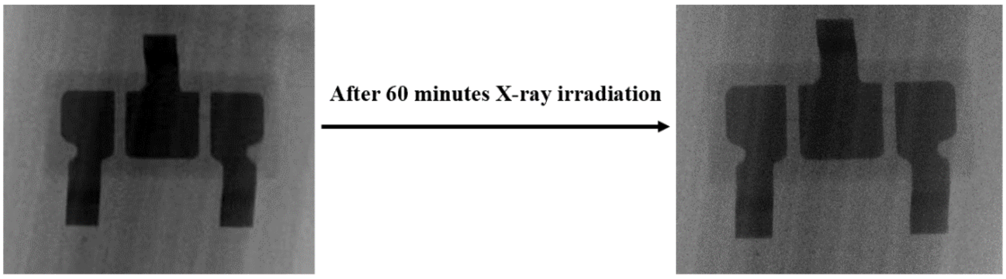

Figure S11 Luminescent photos of the $(C_6H_{10}N_2)_2Cu_2I_3(PO_2)_3$ powder before and after continuous X-ray exposure.

4. Supporting tables

Table S1 The crystal structure parameters of $(C_6H_{10}N_2)_2Cu_2I_3(PO_2)_3$ single crystals.

Compound	$(C_6H_{10}N_2)_2Cu_2I_3(PO_2)_3$
Sum formula	$C_{24}H_{40}N_8Cu_4I_6P_6O_{12}$
Formula Weight	1834.02
$D_{calc.}$**/ g cm^{-3}**	2.366
***Temperature*/K**	293
Crystal System	orthorhombic
Space Group	Pbam
***a*/Å**	13.926 (1)
***b*/Å**	13.9954 (10)
***c*/Å**	13.2077 (10)
α/°	90
β/°	90
γ/°	90
V/Å^3	2574.2 (3)
Z	2
Wavelength/Å	0.71073

μ (mm^{-1})	5.470
F (000)	1720.0

Table S2 Comparison of reported scintillation properties of metal halide perovskites.

Material	PLQY	Scintillation light yield (photons MeV^{-1})	Detection limit (μGy_{air} s^{-1})	Ref.
$(C_6H_{10}N_2)_2Cu_2I_3(PO_2)_3$	**96.4%**	**32,000**	**0.039**	**This work**
$(TBA)Cu_2I_4$	72.5%	/	/	4
$[BAPMA]Cu_2Br_5$	53.4%	43,744	0.074	5
$C_9H_{20}NCuBrI$	99.5%	25,000	0.04	6
$(Bmpip)_2Cu_2Br_4$	48.2%	16,000	0.71	7
$(TBA)CuCl_2$	92.8%	23,373	/	8
$(DIET)_3Cu_3Cl_3$	39.3%	6,000	5.5	9
β-$Cs_3Cu_2I_5$	94.6%	34,000	0.1746	10
$(C_8H_{20}N)_2Cu_2Br_4$	99.7%	91,300	0.052	11
$[AEP]_2Cu_2I_6\cdot 2I\cdot 2H_2O$	97.2%	55,650	/	12

Reference

1. O. Dolomanov, L. Bourhis, R. Gildea, J. Howard and H. P. Olex, *J. Appl. Cryst.*, 2009, **42**, 339-341.
2. L. J. Bourhis, O. V. Dolomanov, R. J. Gildea, J. A. Howard and H. Puschmann, *Acta Cryst.*, 2015, **71**, 59-75.
3. G. M. Sheldrick, *Acta Cryst.*, 2008, **64**, 112-122.
4. H. Peng, Y. Xiao, Y. Tian, X. Wang, T. Huang, T. Dong, Y. Zhao, J. Wang and B. Zou, *J. Mater. Chem. C*, 2021, **9**, 16014-16021.
5. Y.-H. Liu, N.-N. Wang, M.-P. Ren, X. Yan, Y.-F. Wu, C.-Y. Yue and X.-W. Lei, *ACS Appl. Mater. Interfaces*, 2023, **15**, 20219-20227.
6. P. Mao, Y. Tang, B. Wang, D. Fan and Y. Wang, *ACS Appl. Mater. Interfaces*, 2022, **14**, 22295-22301.
7. T. Xu, Y. Li, M. Nikl, R. Kucerkova, Z. Zhou, J. Chen, Y.-Y. Sun, G. Niu, J. Tang and Q. Wang, *ACS Appl. Mater. Interfaces*, 2022, **14**, 14157-14164.
8. L. Lian, X. Wang, P. Zhang, J. Zhu, X. Zhang, J. Gao, S. Wang, G. Liang, D. Zhang and L. Gao, *J. Phys. Chem. Lett.*, 2021, **12**, 6919-6926.
9. K. Han, J. Jin, B. Su, J. Qiao and Z. Xia, *Adv. Opt. Mater.*, 2022, **10**, 2200865.

10. Q. Zhou, J. Ren, J. Xiao, L. Lei, F. Liao, H. Di, C. Wang, L. Yang, Q. Chen and X. Yang, *Nanoscale*, 2021, **13**, 19894-19902.
11. B. Su, J. Jin, K. Han and Z. Xia, *Adv. Funct. Mater.*, 2023, **33**, 2210735.
12. J. H. Wei, Y. W. Yu, J. B. Luo, Z. Z. Zhang and D. B. Kuang, *Adv. Opt. Mater.*, 2022, **10**, 2200724.